

## Is BZB J1450+5201 the most distant gamma-ray BL Lacertae object? \*

Neng-Hui Liao<sup>1,2,3</sup>, Jin-Ming Bai<sup>1,2</sup>, Jian-Guo Wang<sup>1,2</sup>, Hong-Tao Liu<sup>1,2</sup>,  
Jiu-Jia Zhang<sup>1,2,3</sup>, Ning Jiang<sup>4,5</sup>, Zun-Li Yuan<sup>1,2</sup> and Liang Chen<sup>6</sup>

<sup>1</sup> Yunnan Observatories, Chinese Academy of Sciences, Kunming 650011, China;  
*liaonh@ynao.ac.cn; baijinming@ynao.ac.cn*

<sup>2</sup> Key Laboratory for the Structure and Evolution of Celestial Objects, Chinese Academy of Sciences, Kunming 650011, China

<sup>3</sup> University of Chinese Academy of Sciences, Beijing 100049, China

<sup>4</sup> Key Laboratory for Research in Galaxies and Cosmology, University of Science and Technology of China, Chinese Academy of Sciences, Hefei 230026, China

<sup>5</sup> Department of Astronomy, University of Science and Technology of China, Hefei 230026, China

<sup>6</sup> Key Laboratory for Research in Galaxies and Cosmology, Shanghai Astronomical Observatory, Chinese Academy of Sciences, Shanghai 200030, China

Received 2014 February 10; accepted 2014 June 6

**Abstract** BL Lacertae (BL Lac) objects at high redshifts ( $z \geq 2$ ) are rarely detected. Through careful analysis of its Sloan Digital Sky Survey spectrum, BZB J1450+5201 is confirmed to be a high- $z$  BL Lac object with  $z \geq 2.471$  by identifying the Ly $\alpha$  1216 and CIV 1548/1550 absorption lines. This indicates that BZB J1450+5201 is the most distant BL Lac object discovered to date. Careful analysis of the five-year *Fermi*-LAT data of 2FGL J1451.0+5159 shows that its  $\gamma$ -ray emission is robust with a confidence level of  $6.2\sigma$  at 1–3 GeV and  $6.7\sigma$  at 3–10 GeV. This analysis with the five-year data overcomes confusion with its bright neighbor, which is a problem when analyzing the two-year data. In addition, 2FGL J1451.0+5159 is confirmed to be associated with BZB J1450+5201 using the five-year data. The analysis of multiwavelength data, from radio to  $\gamma$ -ray energies, indicates that BZB J1450+5201 is an intermediate synchrotron peaked (ISP) source. Its multiwavelength properties are consistent with distributions of other ISP sources at lower redshifts in the second *Fermi*-LAT AGN catalog. The pure synchrotron self-Compton (SSC) model seems to be disfavored, but the scattering of weak external emission plus the SSC process can provide a satisfactory description of the broadband emission.

**Key words:** galaxies: active — BL Lacertae objects: individual (BZB J1450+5201)  
— gamma rays: galaxies — radiation mechanisms: non-thermal

---

\* Supported by the National Natural Science Foundation of China.

## 1 INTRODUCTION

Blazars, including BL Lacertae (BL Lac) objects and flat spectrum radio quasars (FSRQs) (Urry & Padovani 1995), are radio-loud active galactic nuclei (AGNs) whose relativistic jets are viewed at a small angle with respect to the line of sight (Blandford & Rees 1978). Their broadband radiations are dominated by strongly boosted jet emissions, making them visible at high redshifts. The spectral energy distribution (SED) of a blazar is comprised of two bumps in the  $\log \nu F_\nu - \log \nu$  representation. The first bump, which peaks at UV/X-rays in high-frequency peaked BL Lac objects (HBLs; Padovani & Giommi 1995) and at IR/optical wavelengths in low-frequency peaked BL Lac objects (LBLs) and FSRQs, is widely considered to be synchrotron emission from the relativistic population of electrons. On the other hand, the second bump, which peaks at  $\gamma$ -ray energies, could be interpreted as inverse Compton emission from relativistic electrons up-scattering soft photons. These electrons are in the same population of electrons that generate the first bump. The soft photons could be from the synchrotron emission inside the jet (the synchrotron self-Compton (SSC) model (Maraschi et al. 1992)), or from external photon fields (the external Compton (EC) models: the accretion disk radiation (Dermer & Schlickeiser 1993); UV emission from the broad line region (BLR) (Sikora et al. 1994); or infrared emission from a dust torus (Błażejowski et al. 2000)).

Two classes of blazars dominate the objects in the Second Catalog of AGN (2LAC; Ackermann et al. 2011, hereafter A11) detected by *Fermi*-LAT (Atwood et al. 2009). BL Lac objects are found to outnumber (by a factor  $>3$ ) FSRQs, particularly above 10 GeV (Paneque & The Fermi-LAT Collaboration 2013) because of their harder spectra at GeV-TeV energies. The interactions between the high-energy radiations from high- $z$  BL Lac objects and their surrounding photon fields provide us with an opportunity to measure the  $\gamma$ -ray opacity of the universe and the extragalactic background light (EBL) (e.g. Abdo et al. 2010a). The existence of a strong anticorrelation between the bolometric luminosity and the peak frequency of the synchrotron bump, the so-called the blazar sequence, has been the subject of intense discussions (Fossati et al. 1998; Ghisellini et al. 1998). However, contrasting works have claimed that the sequence could be a selection effect (e.g. Giommi et al. 2012). Recently, the discovery of high- $z$  BL Lac objects with blue synchrotron peaks and high radio luminosities, puts the blazar sequence into a wider context (Padovani et al. 2012; Ghisellini et al. 2012).

The discovery of high- $z$   $\gamma$ -ray BL Lac objects is helpful in understanding the physics of blazars and the blazar sequence. However, high- $z$   $\gamma$ -ray BL Lac objects are rarely detected. The redshift of nearly half of the BL Lac objects in 2LAC is unknown. In fact, the redshift of BL Lac objects is hard to estimate because of their featureless, power-law optical spectra (Marcha et al. 1996; Healey et al. 2007). This severely hampers the study of physics related to blazars. Rau et al. (2012) estimate the photometric redshift of 75 BL Lac objects in 2LAC without a known redshift and find that the highest redshift in their sample is  $z_{\text{sp}} \simeq 1.9$ . Using follow-up spectra and/or archived Sloan Digital Sky Survey (SDSS) spectra, Shaw et al. (2013) (hereafter shaw13) obtain the spectroscopic redshifts or lower redshift limits for most of the BL Lac objects in the 2LAC. They identify that BZB J1450+5201 is a high- $z$  BL Lac object with  $z_{\text{sp}} = 2.471$ . BZB J1450+5201 was first discovered in a damped  $\text{Ly}\alpha$  survey of SDSS Data Release (DR) 3 and was named SDSS J145059.99+520111.7 (Prochaska et al. 2005). From a combination of SDSS DR5 spectroscopy and the Faint Images of the Radio Sky at Twenty cm (FIRST) survey, it was classified as a “higher-confidence” BL Lac candidate (Plotkin et al. 2008). Then it was collected in Roma-BZCAT and flagged as a BL Lac object, named BZB J1450+5201 (Massaro et al. 2009). In fact, the redshift estimation and the  $\gamma$ -ray detection of BZB J1450+5201 need further investigations. Although the redshift of BZB J1450+5201 reported in shaw13 is  $z=2.471$ , it is marked as a special case. Measured values of its redshift that are reported in different data releases vary from 0.435 to 2.47 (e.g. Richards et al. 2009; Plotkin et al. 2010). In addition, its  $\gamma$ -ray emission needs to be checked, because this emission could be contaminated by its bright neighbor in the analysis of two year *Fermi*-LAT data.

In this work, we report a detailed study of the redshift estimate,  $\gamma$ -ray emission detection and multiwavelength properties of BZB J1450+5201, and attempt to constrain its physical parameters. The paper is organized as follows.

In Section 2, we describe the follow-up spectroscopic observation and data reduction, as well as the reduction of LAT data. In Section 3, we describe the careful analysis of its optical and  $\gamma$ -ray data and the main results. The possible nature of BZB J1450+5201 is discussed in Section 4. A short conclusion is listed in Section 5.

Throughout this paper, we adopt a cosmology with  $H_0 = 70 \text{ km s}^{-1} \text{ Mpc}^{-1}$ ,  $\Omega_m = 0.3$  and  $\Omega_\Lambda = 0.7$ . We refer to a spectral index  $\alpha$  as the energy index such that  $F_\nu \propto \nu^{-\alpha}$ , corresponding to a photon index  $\Gamma_{\text{ph}} = \alpha + 1$ .

## 2 OBSERVATIONS AND DATA REDUCTION

### 2.1 Spectroscopic Observations and Data Reduction

Our spectroscopic observation of this object was performed on 2014 April 21 with the Yunnan Faint Object Spectrograph and Camera (YFOSC) mounted on the Lijiang 2.4-m telescope administered by Yunnan Observatories. The YFOSC observation system has been equipped with a  $2.1\text{k} \times 4.5\text{k}$  back-illuminated, blue sensitive CCD, which works in both imaging and long-slit spectroscopic modes (see Zhang et al. 2012 for detailed descriptions of the YFOSC). In imaging mode, the CCD has a field of view of  $9.6' \times 9.6'$  (corresponding to an angular resolution of  $0.28''$  per pixel).

One exposure with a length of 3600 s was taken with grism 8, covering  $\lambda \sim 3600 - 7460 \text{ \AA}$  with a spectral resolution around 2000. The spectrum was reduced using standard IRAF routines, including the corrections for bias, flat field and the removal of cosmic rays. The spectrum was flux-calibrated with spectrophotometric flux from a standard star observed at a similar air mass on the same night. The spectrum was further corrected for atmospheric extinction of the continuum at the Lijiang Observatory. Moreover, telluric lines were also removed from the data. The sky light in the red part could not be removed cleanly because of the poor signal-to-noise ratio (S/N).

### 2.2 Fermi-LAT Data Reduction

The Pass 7  $\gamma$ -ray data for 2FGL J1451.0+5159 were downloaded from the LAT data server.  $\gamma$ -ray photon events, with a time range from 2008 August 4 to 2013 August 4 and an energy range from 0.1 to 300 GeV, were selected. The LAT data were analyzed by the updated standard *ScienceTools* software package version v9r31p1 and the instrument response functions are *P7SOURCE\_V6*. For the LAT background files, we adopted *gal\_2yearp7v6\_v0.fits* as the galactic diffuse model and *iso\_p7v6source.txt* as the isotropic spectral template. The entire data set was filtered with *gtselect* and *gtmktime* tasks by following the standard analysis threads. Only events belonging to class 2 were considered. We used the unbinned likelihood algorithm (Mattox et al. 1996) implemented in the *gtlike* task to extract the flux and spectrum. The *gtfindsrc* task was adopted to locate the position of the  $\gamma$ -ray emission. All sources from the second *Fermi*-LAT catalog (2FGL; Nolan et al. 2012) within  $15^\circ$  of the source position were included. Parameters of sources within the  $10^\circ$  “region of interest” (ROI) were allowed to vary, while parameters of sources that fell outside the ROI were fixed with the values given by 2FGL. During the fitting process, if test statistic (TS) values of the background sources were negative, they were removed in the source model file. Furthermore, exotic parameters from the background sources reaching their limit sets were also fixed at the 2FGL values. If the TS value of the fitting was lower than 4 ( $\simeq 2\sigma$ ), flux was set at the  $2\sigma$  upper limits. All errors reported in the figures or quoted in the text for  $\gamma$ -ray flux are  $1\sigma$  statistical errors, and the error radius of the  $\gamma$ -ray location corresponds to the 68% confidence level.

### 3 RESULTS

#### 3.1 Redshift Re-justification

Redshift measurements of BL Lac objects are difficult because of their featureless spectra. The redshift of BZB J1450+5201 reported in different data releases can change from 0.435 to 2.47. We perform a detailed analysis of SDSS archival spectroscopic data. We re-identify the redshift of this object using the spectrum from SDSS DR7 (Abazajian et al. 2009). We find that the  $\text{Ly}\alpha$  forest and CIV1548/1550 absorption lines, and the CIV doublet absorption lines, are at the onset of the  $\text{Ly}\alpha$  forest. Fortunately, the onset  $\text{Ly}\alpha$  absorption line does not obviously blend with others in the forest, so we can identify the redshift of the absorber according to the  $\text{Ly}\alpha$ 1216 and CIV1548/1550 absorption lines.

To measure the redshift and to estimate the confidence level of these absorption lines, the spectra are corrected for Galactic extinction using the extinction map of Schlegel et al. (1998) and the reddening curve of Fitzpatrick (1999). The power-law continuum and three absorption lines (one Gaussian for each absorption line) are fitted simultaneously. The CIV doublets are assumed to have the same width. The measured redshift,  $z = 2.471 \pm 0.002$ , is the same for shaw13, as shown in Figure 1. The uncertainty in redshift is estimated from the uncertainty in the position of the valley shown by absorption lines. For each absorption line, the equivalent width (EW) is measured in the  $\pm 2\sigma$  width around the center wavelength and the error of EW is measured from the error spectrum in the same interval. For the  $\text{Ly}\alpha$ 1216 and CIV1548/1550 absorption lines, the EWs are  $1.26 \pm 0.17 \text{ \AA}$ ,  $0.49 \pm 0.15 \text{ \AA}$  and  $0.45 \pm 0.14 \text{ \AA}$  respectively. The corresponding confidence levels are  $7.2\sigma$ ,  $3.3\sigma$  and  $3.1\sigma$ .

There are several potential absorption and emission lines in the red part of the SDSS spectrum. We cannot judge whether they are real absorption/emission lines or artificial absorption/emission lines due to residuals from sky subtraction (Wild & Hewett 2005), so we take a follow-up spec-

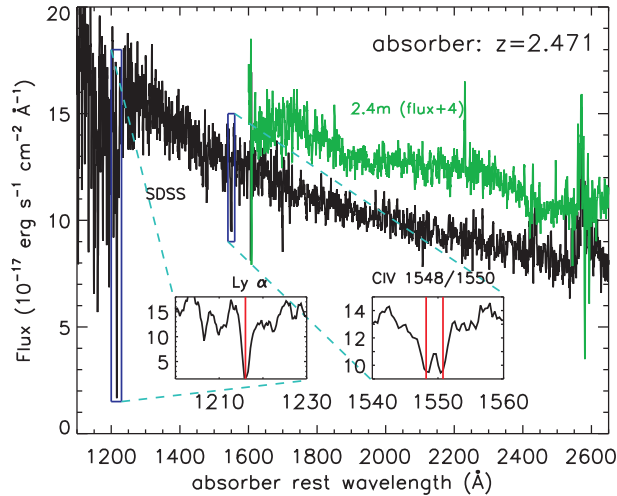


**Fig. 1** The YFOSC and SDSS spectra. The black spectrum of BZBJ1450+5201 from SDSS DR7 was smoothed with a 4-pixel boxcar filter. The wavelength is at the rest frame of the absorber with a redshift of 2.471. The inset shows the  $\text{Ly}\alpha$  line and CIV 1548/1550 doublets. The green spectrum represents the YFOSC spectrum taken from our follow-up observation with the 2.4-m telescope at Yunnan Observatories.

troscopic observation of this object using YFOSC mounted on the 2.4-m telescope at Yunnan Observatories. The YFOSC spectrum is also shown in Figure 1. The S/N at each tip of the YFOSC spectrum is poor because the object is faint and the efficiency of the grism there is relatively low, so these parts of the spectrum are not shown in Figure 1. We confirm that there is no obvious absorption or emission line in the red part of the spectrum. Most of the absorption and emission lines on the red part of both the SDSS and YFOSC spectra are caused by the poor reduction of sky light because of the low S/N of the spectra. Therefore, a redshift of 2.47 is adopted throughout this paper.

Besides BZB J1450+5201, there are several high- $z$  BL Lac objects that have been reported in the literature. The redshift of BZB J0508+8432 has been reported as  $z_{\text{sp}}=1.340$  (Urry et al. 2000). The redshift of BZB J1642–0621, whose  $\gamma$ -ray emission has been detected by LAT, has been identified as  $z_{\text{sp}}=1.514$  (Sowards-Emmerd et al. 2004). However, this estimate has been marked as “marginal” due to the identification by a single line or spectrum with a low S/N. The redshift of another BL Lac object, BZB J0039+1411, has been suggested to be  $z_{\text{sp}}=1.715$  (Sowards-Emmerd et al. 2005; Healey et al. 2008). Recently, the photometric redshift of BZB J0402–2615 has been given as  $z_{\text{ph}}=1.920$  (Rau et al. 2012).

In the shaw13 sample, besides BZB J1450+5201, there is another BL Lac object, BZB J0124–0625, whose redshift is greater than 2 ( $z_{\text{sp}}=2.117$ ). This estimate is based on a single strong feature shown by [O II], which is consistent with weak MgII and Ca H/K absorptions. Like BZB J1450+5201, BZB J0124–0625 has been marked as a special case in shaw13. As mentioned below, if the redshift of BZB J1450+5201 is indeed 2.471, it would be the most distant BL Lac object discovered so far.

### 3.2 Validation of $\gamma$ -ray Emission from BZB J1450+5201

#### 3.2.1 Removal of the data flag in 2FGL

Due to the brighter source within  $1^\circ$  from the target, when analyzing its  $\gamma$ -ray emission one should be cautious. In both the 2FGL and first *Fermi*-LAT catalog (1FGL, Abdo et al. 2010b), the highest TS values are detected at 1–3 GeV, as shown in Table 1.

The adopted reference distance,  $\theta_{\text{ref}}$ , should be that at 1–3 GeV according to the criteria used in 1FGL and 2FGL, which is defined in the highest band of a source in which the value of TS  $> 25$  or the band with the highest TS if all are  $< 25$  (Nolan et al. 2012). The angular separation ( $\simeq 0.8^\circ$ ) between 2FGL J1450+5201 and its bright neighbor is comparable with the  $\theta_{\text{ref}}$  at 1–3 GeV ( $\simeq 0.8^\circ$ ).

**Table 1**  $\gamma$ -ray Locations and TS Values at Five Energy Bands of BZB J1450+520 from 1FGL, 2FGL and Five-year Analyses

	1FGL J1451.0+5204	2FGL J1451.0+5159	5-year analysis
R.A. (J2000)	222.7679 $^\circ$	222.751 $^\circ$	222.737 $^\circ$
Dec. (J2000)	52.0685 $^\circ$	51.9913 $^\circ$	52.0216 $^\circ$
$r$ (68%)	0.094 $^\circ$	0.053 $^\circ$	0.037 $^\circ$
$\Delta r$	0.05 $^\circ$	0.03 $^\circ$	0.008 $^\circ$
$\Delta r'$	0.847 $^\circ$	0.801 $^\circ$	0.844 $^\circ$
TS_100_300	0	0.3	0
TS_300_1000	3.4	13.3	22.2
TS_1000_3000	26.6	16.9	38.7
TS_3000_10000	7.5	13.8	45.5
TS_10000_100000	0	10.1	16.2

Notes: R.A./Dec. – right ascension/declination of the  $\gamma$ -ray localization;  $r$  (68%) – 68% confidence level for geometric mean localization error radius;  $\Delta r$  – angular separation of respective radio source position;  $\Delta r'$  – angular separation of nearby brighter  $\gamma$ -ray source position; TS – likelihood test statistic value.

The contamination from the bright neighbor may influence the confidence level of  $\gamma$ -ray detection. 2FGL J1450+5201 is a marginal case and has not been included in the clean sample.

Therefore, we analyze the five-year data of Fermi LAT and check whether the associated confidence level would increase using more events. Fortunately, the analysis indicates that the confidence level of 2FGL J1451.0+5159 is high enough with a TS value of 45.5 at 3–10 GeV and 38.7 at 1–3 GeV. Then the adopted  $\theta_{\text{ref}}$  should be that at 3–10 GeV ( $0.67^\circ$ ). The angular separation between it and its bright neighbor is obviously larger than  $\theta_{\text{ref}}$ , as shown in Table 1. 2FGL J1451.0+5159 is a robust  $\gamma$ -ray emitting source.

TS maps for both the energy ranges at 0.1–100 GeV and 3–10 GeV confirm our fitting results, as shown in Figure 2. First, TS maps with the target removed in the model files exhibit prominent sources at the center, whose TS values agree with those obtained from the *glike* analysis. These prominent sources should correspond to the target. In TS maps with both the target and the nearby brighter source removed from the model file, the contribution of the target is perceivable for 3–10 GeV, but the nearby source is totally dominant for 0.1–100 GeV. We also present two residual TS maps with scales of  $10^\circ \times 10^\circ$ , in which the highest TS values are lower than 20. The probability that the  $\gamma$ -ray emission of the target is contaminated by nearby sources absent from the 2FGL is ruled out. However, a new  $\gamma$ -ray candidate probably appears  $6.5^\circ$  away from the target, with a significance of about  $7\sigma$ . The effect of whether the candidate is in or absent from the model file is negligible for the measurement of the  $\gamma$ -ray emission from the target. Nevertheless, adding the candidate into the model file is helpful to clean the residual TS map at 0.1–100 GeV.

With the increase of detected  $\gamma$ -ray events, the uncertainty in position decreased from  $0.053^\circ$  in 2FGL to  $0.037^\circ$ . We confirm the prior conclusion that 2FGL J1451.0+5159 is associated with BZB J1450+5201 (Nolan et al. 2012), as shown in Figure 3. Using the  $\gamma$ -ray luminosity function (LDDE2; Ajello et al. 2014), the expected number of BL Lac objects with  $\gamma$ -ray luminosities above the five-year averaged  $\gamma$ -ray luminosity,  $2.9 \times 10^{47} \text{ erg s}^{-1}$ , and redshifts above 2.47 is estimated to only be  $\sim 0.81_{-0.77}^{+6.28}$ . This indicates that BZB J1450+5201 may be an extraordinary BL Lac object and it may be helpful for understanding the physics of blazars.

### 3.3 Multiwavelength Properties

Multi-wavelength data on BZB J1450+5201 are essential for investigating its properties and restricting possible classification. In the  $\gamma$ -ray domain, a whole fit for the five-year *Fermi*-LAT data, using a power-law as the spectral function, gives the average flux of  $(6.05 \pm 1.55) \times 10^{-9} \text{ ph cm}^{-2} \text{ s}^{-1}$  with the TS value of 112.7 ( $10.6\sigma$ ) and photon index of  $2.03 \pm 0.11$ . The mid-infrared data are obtained by the *Wide-field Infrared Survey Explorer* (*WISE*; Wright et al. 2010) which has mapped the entire sky in four bands centered at 3.4, 4.6, 12 and 22  $\mu\text{m}$  (hereafter the W1, W2, W3 and W4 bands respectively). BZB J1450+5201 is detected with high S/N in all four bands, with a flux density, converted from the magnitudes in the *WISE* All-sky Source Catalog, of  $0.87 \pm 0.02$ ,  $1.23 \pm 0.03$ ,  $2.32 \pm 0.10$  and  $5.06 \pm 0.68 \text{ mJy}$ , respectively. Optical magnitudes are taken from SDSS DR7 (Abazajian et al. 2009). Meanwhile, near-infrared (NIR) photometric data are extracted from Two Micron All Sky Survey (2MASS) catalogs (Skrutskie et al. 2006). The observed optical-NIR magnitudes are converted into flux density (Janskys) using the zero magnitudes from Bessell (2005). These data are corrected for Galactic extinction using the extinction map of Schlegel et al. (1998) and the reddening curve of Fitzpatrick (1999), although the correction is negligible for *WISE* data. We collect radio flux densities from observations of the FIRST survey at 1.4 GHz (White et al. 1997), the VLBA imaging and Polarimetry Survey (VIPS; Helmboldt et al. 2007) at 5 GHz and the Cosmic Lens All-Sky Survey (CLASS; Myers et al. 2003) at 8.5 GHz. The target is classified as a point source in the radio image study with the bright core temperature of  $\sim 2 \times 10^{10} \text{ K}$  (Linford et al. 2012). No source has been found within  $5'$  of the source position in the ROSAT All-Sky Survey Faint Source Catalogue (Voges et al. 2000).

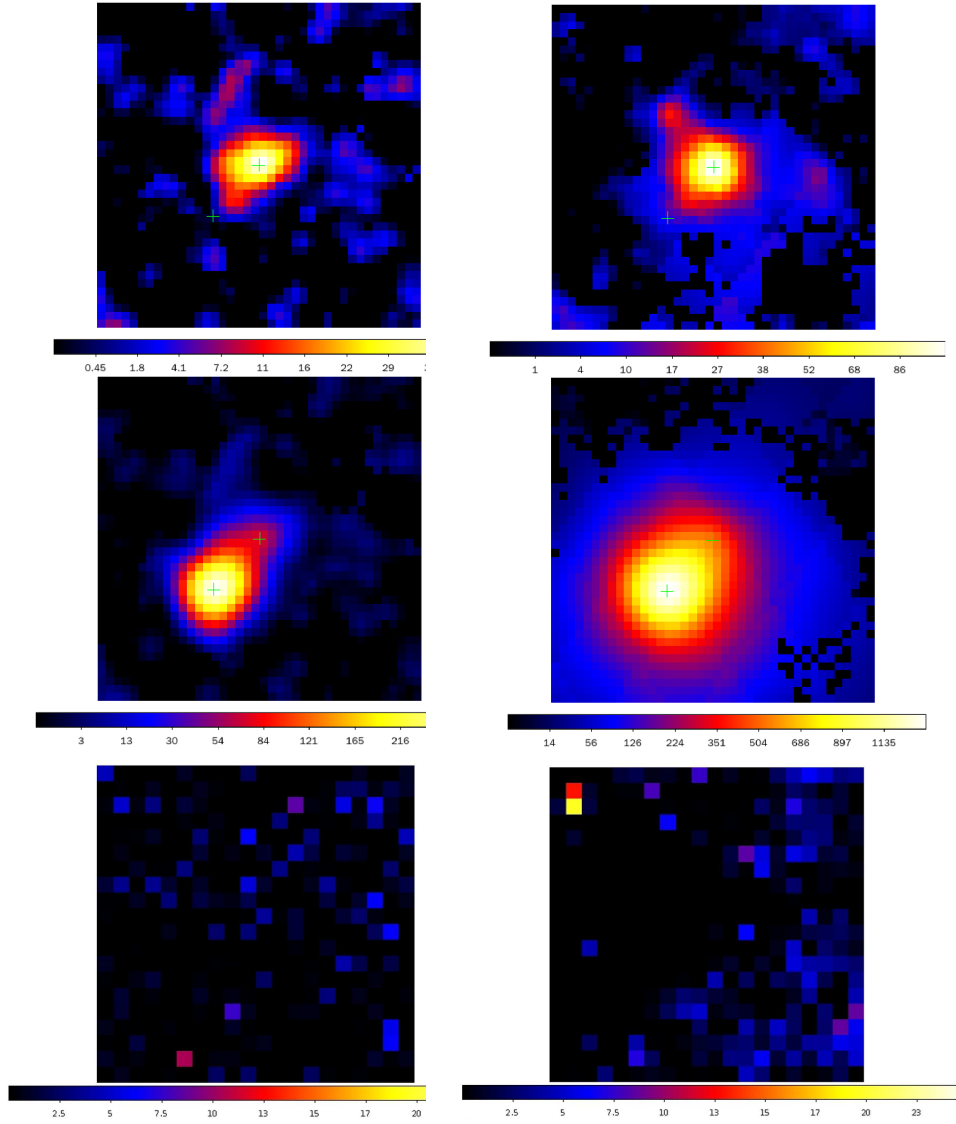


**Fig. 2** TS maps centered at the five-year  $\gamma$ -ray position of BZB J1450+520. The left and right panels correspond to the energy ranges 3–10 GeV and 0.1–100 GeV, respectively. TS maps with only the target removed from the model files are presented in the top panels. Middle panels correspond to TS maps with both the target and brighter neighbor removed from the model files. The plus signs show locations of the target and the neighbor. The bottom panels are residual TS maps on a scale of  $10^\circ \times 10^\circ$ , with one pixel corresponding to  $0.2^\circ$ .

### 3.3.1 EBL-related $\gamma$ -ray absorption optical depth

Detections of high energy photon events of large EBL-related opacity are usually used to test the EBL estimate. Recently, such events from two  $\gamma$ -ray BL Lac objects have been reported. One object

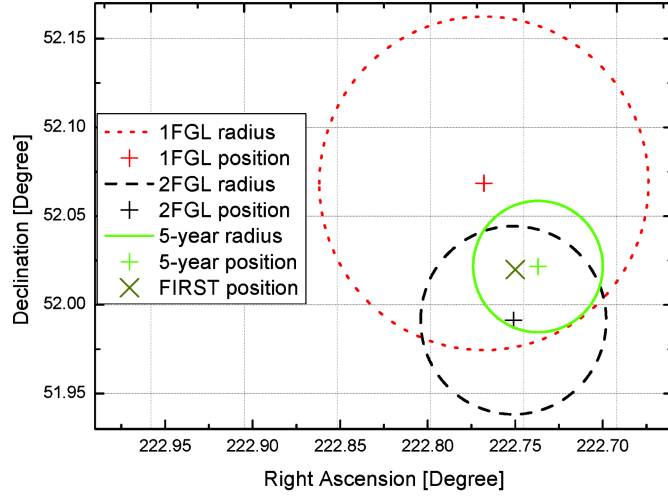


**Fig. 3**  $\gamma$ -ray locations of BZB J1450+520 from 1FGL, 2FGL and five-year analyses with corresponding error radii, together with its radio position.

is PKS 0426–380. Two very high energy (VHE)  $\gamma$ -ray photons, 134 and 122 GeV, have been detected recently (Tanaka et al. 2013). The redshift of this source is  $z_{\text{sp}} = 1.1$  (Sbarufatti et al. 2005), which is just around the horizon for  $\simeq 100$  GeV  $\gamma$  rays. (EBL absorption optical depth  $\tau_{\gamma\gamma} \simeq 1$ ) (Ackermann et al. 2012). The other is PKS 1424+240. The lower limit of its redshift is  $z_{\text{sp}} \geq 0.6035$  by analyzing the far-ultraviolet spectra (Furniss et al. 2013). VHE observations of PKS 1424+240 out to energies of 500 GeV have been detected by VERITAS (Acciari et al. 2010). Corresponding to this redshift lower limit, the EBL optical depth for VHE  $\gamma$ -ray photons of 500 GeV is  $\tau_{\gamma\gamma} \simeq 5$  which puts a severe challenge on the current EBL models.

In BZB J1450+5201, as the most distant gamma-ray BL Lac object, the absorption optical depth would be large if some photons with high enough energy are detected. We searched the highest energy photon events of BZB J1450+5201 by using the task *gtsrcprob*. One photon event is 16.9 GeV and the other is 17.6 GeV, with probabilities of 98.6% and 98.3%, respectively. Adopting several EBL models (Finke et al. 2010; Stecker et al. 2012), the corresponding optical depth of photons with energy around 17 GeV is  $\tau_{\gamma\gamma} \simeq 0.1$ . Therefore, the detections will not challenge the present EBL estimate.

### 3.3.2 Constraints on the peak frequencies and luminosities of the SED bumps

The peak frequencies and luminosities are important for understanding the classification of blazars and the parameters of the emission model. Besides the whole fit of the *Fermi*-LAT data, we extract the averaged  $\gamma$ -ray spectrum with the python script *likeSED* from *Fermi*-LAT user contributions. Due to the relatively large errors in the spectrum, we do not find any evidence of significant spectral curvature. However, the  $\gamma$ -ray photon index is close to 2, indicating that the peak frequency of the second SED bump may be within the spectrum. So, we perform a LogParabola fit for the averaged spectrum, which provides restrictions on the peak frequency and luminosity of the second bump,  $10^{24.32 \pm 0.58}$  Hz and  $10^{46.74 \pm 0.08}$  erg s $^{-1}$ , respectively. For the first bump, the IR-optical data from *WISE*, 2MASS and SDSS are also fitted by the LogParabola function to restrict its peak frequency and luminosity, which are  $\nu_{\text{peak}}^{\text{syn}} = 10^{14.74 \pm 0.02}$  Hz and  $L_{\text{peak}}^{\text{syn}} = 10^{46.608 \pm 0.005}$  erg s $^{-1}$ , respectively. According to the value of its synchrotron peak frequency, BZB J1450+5201 is classified as

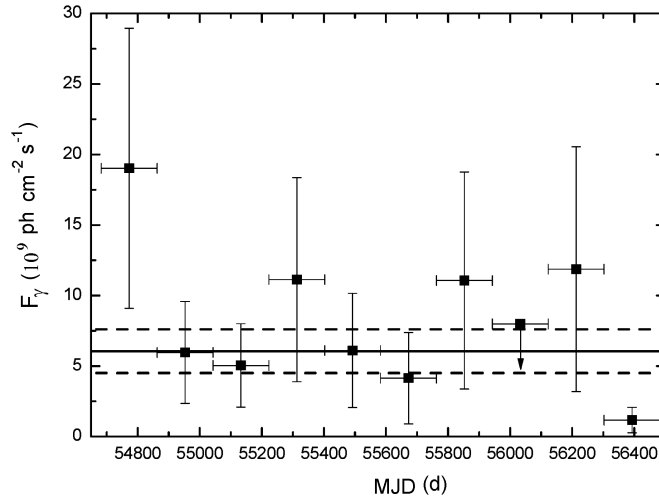


**Fig. 4**  $\gamma$ -ray light curve with a time bin of six months. The solid horizontal line corresponds to the average flux whose  $1\sigma$  error is presented as dashed lines.

an intermediate synchrotron peaked (ISP) blazar (Abdo et al. 2010c). Together with the  $\Gamma_\gamma \simeq 2$ , the source falls into the region filled by the ISP blazars of 2LAC in the  $\Gamma_\gamma - \nu_{\text{peak}}^{\text{syn}}$  diagram (see fig. 17 in A11). As the five-year average  $\gamma$ -ray luminosity is about  $2.9 \times 10^{47} \text{ erg s}^{-1}$ , the source does not deviate from the  $\Gamma_\gamma - L_\gamma$  distribution shown by ISP blazars in 2LAC (see fig. 37 in A11). A correlation between the Compton Dominance (CD) and  $\nu_{\text{peak}}^{\text{syn}}$  is found for 2LAC blazars (Finke 2013). For BZB J1450+5201, the CD value is about 1.4, together with the  $\nu_{\text{peak}}^{\text{syn}}$  of about  $10^{14.7} \text{ Hz}$ , indicating that the source has the same tendency as presented in Finke (2013). It seems that BZB J1450+5201 is no different from other ISP blazars in 2LAC except for the high redshift.

### 3.3.3 Variability in $\gamma$ -ray and infrared energies

Although BZB J1450+5201 is faint in the  $\gamma$ -ray domain, we attempt to extract its  $\gamma$ -ray light curve with a six-month time bin, which can be used to investigate the  $\gamma$ -ray variability on a long timescale, as shown in Figure 4. We use the  $\chi^2$  test to check whether the source exhibits significant variability (Abdo et al. 2010d). It is suggested that the light curve deviates from the distribution of a constant flux with probability of only about 83%. We also use “normalized excess variance” ( $\sigma_{NXS}^2$ ) to quantify the variability amplitude (Edelson et al. 2002). No significant variability is detected.

In IR bands, the observing cadence of *WISE* is well suited for studying intraday variability, typically with 12 successive orbits covering a given source in one day (see Hoffman et al. 2012). There are around 25 exposures in two days for J1450+5201. The photometric errors of the *WISE* data have been examined using SDSS Stripe 82 standard stars (Jiang et al. 2012). With the contribution from measurement errors subtracted, the variability amplitude is measured by the variance of the observed magnitudes (Sesar et al. 2007). Unfortunately, no significant variability is detected.

## 4 DISCUSSION

Using the obtained multi-wavelength data, we attempt to put constraints on the physical parameters of the source. The classic synchrotron plus SSC model is first adopted. The multi-wavelength emission is assumed to be from the same population of relativistic electrons with a broken power-law

distribution. The influence of the Klein-Nishina effect is calculated, which is negligible for  $\gamma$ -ray emission from the source. The constraints on the magnetic field intensity  $B$  and Doppler factor  $\delta$  are calculated using equations from Tavecchio et al. (1998)

$$B\delta = (1+z) \frac{\nu_{\text{syn}}^2}{2.8 \times 10^6 \nu_{\text{SSC}}}, \quad (1)$$

$$B\delta^3 \geq (1+z) \left\{ \frac{2L_{\text{syn}}^2 f}{c^3 t_{\text{var}}^2 L_{\text{SSC}}} \right\}^{1/2}, \quad (2)$$

where  $f = \frac{1}{1-\alpha_1} + \frac{1}{\alpha_2-1}$  and  $R \leq c\delta t_{\text{var}}(1+z)^{-1}$  are adopted. The spectral indexes  $\alpha_{1,2}$  are obtained by fitting the *WISE* and SDSS data, which are 0.5 and 1.5, respectively.  $\alpha_1 = 0.5$  and  $\alpha_2 = 1.5$ . If the typical variability timescale, one day, is adopted, the resultant Doppler factor would be too large,  $\delta \simeq 145$ , and the corresponding magnetic field intensity would be  $B \simeq 1 \times 10^{-3}$  G. These parameter values are not acceptable. Because no evidence of significant flux variations in  $\gamma$ -ray or IR energies is detected,  $t_{\text{var}}$  of 30 days is adopted to re-calculate these parameters. The value of the Doppler factor is reduced to  $\delta \simeq 27$  which is consistent with the typical value from kinematic studies of blazars. Then, the magnetic field intensity is  $B \simeq 7 \times 10^{-3}$  G. Such a low value of magnetic field intensity does not agree with the typical value from similar previous SED fitting works (e.g. Liao et al. 2014). The pure SSC model is probably disfavored. Since evidence of intraday variability in the optical band for several ISP blazars has been reported (e.g. Chandra et al. 2011), the detection of potential intraday variability for BZB J1450+5201 in the future would severely challenge the pure SSC model.

Similar to BZB J1450+5201, other studies on the SEDs of ISP blazars (e.g. Abdo et al. 2011b; Liao et al. 2014) also suggest that the pure SSC model is disfavored and that SSC plus EC models are acceptable. Therefore, we adopt the SSC plus EC model that assumes relativistic electron scattering from BLR emission. These external target photons are approximated as blackbody emission peaking at the frequency of the Ly $\alpha$  line. This model can well represent the SED as shown in Figure 5.

The modeling parameters are as follows: radiation emission radius  $R \simeq 2.2 \times 10^{16}$  cm; Doppler factor  $\delta \simeq 29$ ; magnetic field intensity  $B \simeq 0.3$  G; energy density of BLR emission in the rest frame  $U_{\text{BLR}} \simeq 4.2 \times 10^{-5}$  erg cm $^{-3}$ ; energy break in the electron distribution  $\gamma_{\text{br}} \simeq 4.2 \times 10^3$ ; spectral indexes of the electron distribution  $p_1 = 2$  and  $p_2 = 4$ . Because no obvious broad emission line is detected, the size of the BLR is unknown. A typical size for the BLR (0.1 pc) is adopted. Together with the energy density of BLR emission from the SED modeling, the corresponding luminosity of BLR emission does not exceed the jet emission, making our assumption of the BLR emission agree with other results. Assuming that one proton corresponds to one relativistic emitting electron and that protons are ‘cold’ in the comoving frame (Celotti & Ghisellini 2008), the power of the jet is estimated as being about  $6 \times 10^{47}$  erg s $^{-1}$ . If the Blandford-Znajek mechanism (Blandford & Znajek 1977) is mainly responsible for launching the jet (Paggi et al. 2009), then  $P_{\text{jet}} \leq P_{\text{BZ}}$ . Using the method in Levinson (2006), a gross estimate of the mass of the central black hole is  $M_{\text{BH}} \geq 7 \times 10^9 M_{\odot}$ , which is on the same order of magnitude as measurements of other high- $z$  blazars (Romani et al. 2004; Sbarrato et al. 2012).

Since the blazar sequence was introduced (Fossati et al. 1998), it has drawn a lot of attention. The sequence can be explained as the result of an inverse correlation between  $\gamma_{\text{p}}$  and the summation of the magnetic and radiative energy densities, where  $\gamma_{\text{p}}$  is the electron energy emitted at the synchrotron peak (e.g. Ghisellini et al. 1998; Ghisellini et al. 2002; Celotti & Ghisellini 2008). However, other explanations have been reported (e.g. Padovani 2007). Recently, an extensive Monte Carlo simulation study, assuming that  $\gamma_{\text{p}}$  is irrelevant to the subclass of blazars, could well represent blazars detected in radio and X-ray surveys (Giommi et al. 2012). They claim that the classification criterion of blazars based on their optical spectra is a selection effect and FSRQs with synchrotron

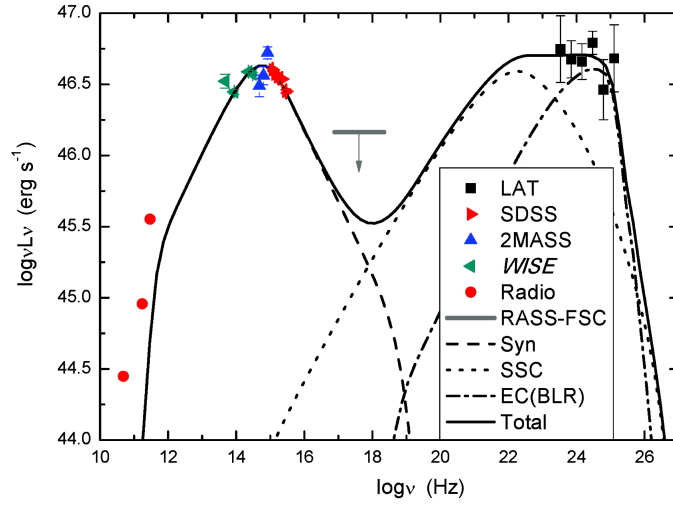


**Fig. 5** SED modeling using synchrotron and SSC plus EC model scattering with assumed BLR emission that comes from external photons. The source of multi-wavelength data has been introduced in Sect. 3.3.

peaks falling at optical/UV energies, where their strong broad emission lines are heavily swamped, are masquerading as BL Lac objects. The radio power has been suggested as a potentially unbiased classification criterion. Moreover, their Monte Carlo simulation is applicable to the *Fermi*-LAT survey (Giommi et al. 2013). They claim that the *Fermi*-LAT BL Lac objects without redshift estimates, most of which are high synchrotron peaked (HSP) blazars and  $\sim 1/3$  are Intermediate Synchrotron Peaked (ISP) blazars, are probably FSRQs. Recent studies of individual sources seem to support their simulation results. Four BL Lac objects in 2LAC, with their recently determined photometric redshifts from 1.2 to 1.8,  $\nu_{\text{peak}}^{\text{syn}}$  higher than  $10^{15}$  Hz and strong radio radiations ( $\geq 10^{44}$  erg s $^{-1}$ ), may be a real sample of “Blue FSRQs” predicted in the simulations (Padovani et al. 2012). The SED modeling of these four “Blue FSRQs” indicates that they are indeed FSRQs (Ghisellini et al. 2012).

BZB J1450+5201 looks like those “Blue FSRQs.” Its synchrotron peak is located at optical/UV energies and it generates strong radio radiation,  $L_{5 \text{ GHz}} \simeq 5 \times 10^{44}$  erg s $^{-1}$ . However, we actually do not know whether its external photon fields are intrinsically weak or just diluted. SED modeling provides an effective way to constrain the energy density of the external fields. Besides SSC and EC scattering of the BLR emission, another SSC plus EC model, that has scattering of assumed hot dust emission at 1200 K, is also considered in the SED modeling. The energy density of the dust emission in the rest frame is  $1.1 \times 10^{-6}$  erg cm $^{-3}$ . Both the energy densities of the dust and BLR emissions are two orders of magnitude lower than the typical energy densities of the dust and BLR emissions for FSRQs, which are  $2.7 \times 10^{-4}$  and  $2.7 \times 10^{-2}$  erg cm $^{-3}$ , respectively (Ghisellini et al. 2012). However, the external radiation densities that we estimated are consistent with results of the SED modeling studies of other ISP blazars (S5 0716+714, Rani et al. 2013, Liao et al. 2014; BL Lacertae, Abdo et al. 2011b; 3C 66A, Abdo et al. 2011a; W Comae, Acciari et al. 2009). Several ISP blazars, such as S5 0716+714 and BL Lacertae, not only exhibit weak external radiation densities, but also generate strong radio radiations,  $L_{\text{radio}} \geq 10^{44}$  erg s $^{-1}$ . If the external radiation densities of BZB J1450+5201 are indeed weak, the source may not be an example of “Blue FSRQs.” However, our SED data are non-simultaneous and their variability properties are poorly known. Simultaneous multiwavelength observational campaigns are needed in the future to investigate the nature of BZB J1450+5201.

## 5 CONCLUSIONS

We report a detailed investigation of the redshift estimate,  $\gamma$ -ray emission detection and multiwavelength properties of BZB J1450+5201. An absorber system at  $z=2.471$  including Ly $\alpha$  1216 and CIV 1548/1550 absorption lines is identified by analyzing archival SDSS spectral data, and the results are consistent with the literature. Moreover, we take a follow-up spectroscopic observation covering the red part of the spectrum with the 2.4-m telescope at Yunnan Observatories. Unfortunately, no significant emission or absorption lines can be identified. BZB J1450+5201 is suggested to be the most distant BL Lac object to date. Its  $\gamma$ -ray emission is detected at a high confidence level by analyzing the five-year *Fermi*-LAT data. The highest energy of the detected  $\gamma$ -ray event is  $\simeq 17$  GeV. The corresponding opacity of EBL absorption is  $\tau_{\gamma\gamma} \simeq 0.1$  which is reasonable under the current EBL estimate. BZB J1450+5201 is found to be an ISP blazar and it does not deviate from distributions of other ISP sources at lower redshifts in 2LAC. Like several other ISP blazars, a pure SSC model is likely disfavored, but SSC plus EC scattering of weak external photon fields can well represent the SED. Although BZB J1450+5201 generates strong radio radiation and its synchrotron peak is located at optical/UV energies, if its external radiation densities are intrinsically weak, the source may not be an example of “Blue FSRQs.”

**Acknowledgements** We thank the anonymous referee very much for his/her constructive suggestions which helped to improve the paper a great deal. This research has made use of data obtained from the High Energy Astrophysics Science Archive Research Center, provided by the NASA/Goddard Space Flight Center. This research has also made use of the NASA/IPAC Infrared Science Archive, which is operated by the Jet Propulsion Laboratory, California Institute of Technology, under contract with the National Aeronautics and Space Administration. We thank Seth Digel, Ming Zhou, Ye Li and the *Fermi*-LAT help-group for their suggestions. The authors gratefully acknowledge the computing time granted by Yunnan Observatories, and provided on the facilities at the Yunnan Observatories Supercomputing Platform. This work is financially supported by the National Natural Science Foundation of China (Grant Nos. 11133006, 11273052 and 11103060).

## References

- Abazajian, K. N., Adelman-McCarthy, J. K., Agüeros, M. A., et al. 2009, *ApJS*, 182, 543  
 Abdo, A. A., Ackermann, M., Ajello, M., et al. 2010a, *ApJ*, 723, 1082  
 Abdo, A. A., Ackermann, M., Ajello, M., et al. 2010b, *ApJS*, 188, 405  
 Abdo, A. A., Ackermann, M., Agudo, I., et al. 2010c, *ApJ*, 716, 30  
 Abdo, A. A., Ackermann, M., Ajello, M., et al. 2010d, *ApJ*, 722, 520  
 Abdo, A. A., Ackermann, M., Ajello, M., et al. 2011a, *ApJ*, 726, 43  
 Abdo, A. A., Ackermann, M., Ajello, M., et al. 2011b, *ApJ*, 730, 101  
 Acciari, V. A., Aliu, E., Aune, T., et al. 2009, *ApJ*, 707, 612  
 Acciari, V. A., Aliu, E., Arlen, T., et al. 2010, *ApJ*, 708, L100  
 Ackermann, M., Ajello, M., Allafort, A., et al. 2011, *ApJ*, 743, 171 (A11)  
 Ackermann, M., Ajello, M., Allafort, A., et al. 2012, *Science*, 338, 1190  
 Ajello, M., Romani, R. W., Gasparrini, D., et al. 2014, *ApJ*, 780, 73 (arXiv:1310.0006)  
 Atwood, W. B., Abdo, A. A., Ackermann, M., et al. 2009, *ApJ*, 697, 1071  
 Bessell, M.-S. 2005, *ARA&A*, 43, 293  
 Blandford, R. D., & Znajek, R. L. 1977, *MNRAS*, 179, 433  
 Blandford, R. D., & Rees, M. J. 1978, in *BL Lac Objects*, ed. A. M. Wolfe (Pittsburgh: Univ. Pittsburgh Press), 328  
 Błażejowski, M., Sikora, M., Moderski, R., & Madejski, G. M. 2000, *ApJ*, 545, 107  
 Celotti, A., & Ghisellini, G. 2008, *MNRAS*, 385, 283

- Chandra, S., Baliyan, K. S., Ganesh, S., & Joshi, U. C. 2011, *ApJ*, 731, 118
- Dermer, C. D., & Schlickeiser, R. 1993, *ApJ*, 416, 458
- Edelson, R., Turner, T. J., Pounds, K., et al. 2002, *ApJ*, 568, 610
- Finke, J. D. 2013, *ApJ*, 763, 134
- Finke, J. D., Razzaque, S., & Dermer, C. D. 2010, *ApJ*, 712, 238
- Fitzpatrick, E. L. 1999, *PASP*, 111, 63
- Fossati, G., Maraschi, L., Celotti, A., Comastri, A., & Ghisellini, G. 1998, *MNRAS*, 299, 433
- Furniss, A., Williams, D. A., Danforth, C., et al. 2013, *ApJ*, 768, L31
- Ghisellini, G., Celotti, A., Fossati, G., Maraschi, L., & Comastri, A. 1998, *MNRAS*, 301, 451
- Ghisellini, G., Celotti, A., & Costamante, L. 2002, *A&A*, 386, 833
- Ghisellini, G., Tavecchio, F., Foschini, L., et al. 2012, *MNRAS*, 425, 1371
- Giommi, P., Padovani, P., Polenta, G., et al. 2012, *MNRAS*, 420, 2899
- Giommi, P., Padovani, P., & Polenta, G. 2013, *MNRAS*, 431, 1914
- Healey, S. E., Romani, R. W., Taylor, G. B., et al. 2007, *ApJS*, 171, 61
- Healey, S. E., Romani, R. W., Cotter, G., et al. 2008, *ApJS*, 175, 97
- Helmboldt, J. F., Taylor, G. B., Tremblay, S., et al. 2007, *ApJ*, 658, 203
- Hoffman, D. I., Cutri, R. M., Masci, F. J., et al. 2012, *AJ*, 143, 118
- Jiang, N., Zhou, H.-Y., Ho, L. C., et al. 2012, *ApJ*, 759, L31
- Levinson, A. 2006, in *Trends in Black Hole Research*, 119 (Nova Science Publishers)
- Liao, N. H., Bai, J. M., Liu, H. T., et al. 2014, *ApJ*, 783, 83
- Linford, J. D., Taylor, G. B., Romani, R. W., et al. 2012, *ApJ*, 744, 177
- Maraschi, L., Ghisellini, G., & Celotti, A. 1992, *ApJ*, 397, L5
- Marcha, M. J. M., Browne, I. W. A., Impey, C. D., & Smith, P. S. 1996, *MNRAS*, 281, 425
- Massaro, E., Giommi, P., Leto, C., et al. 2009, *A&A*, 495, 691
- Mattox, J. R., Bertsch, D. L., Chiang, J., et al. 1996, *ApJ*, 461, 396
- Myers, S. T., Jackson, N. J., Browne, I. W. A., et al. 2003, 341, 1
- Nolan, P. L., Abdo, A. A., Ackermann, M., et al. 2012, *ApJS*, 199, 31
- Padovani, P. 2007, *Ap&SS*, 309, 63
- Padovani, P., & Giommi, P. 1995, *ApJ*, 444, 567
- Padovani, P., Giommi, P., & Rau, A. 2012, *MNRAS*, 422, L48
- Paggi, A., Cavaliere, A., Vittorini, V., & Tavani, M. 2009, *A&A*, 508, L31
- Paneque, D., & The Fermi-LAT Collaboration 2013, arXiv:1306.6772
- Plotkin, R. M., Anderson, S. F., Hall, P. B., et al. 2008, *AJ*, 135, 2453
- Plotkin, R. M., Anderson, S. F., Brandt, W. N., et al. 2010, *AJ*, 139, 390
- Prochaska, J. X., Herbert-Fort, S., & Wolfe, A. M. 2005, *ApJ*, 635, 123
- Rani, B., Krichbaum, T. P., Fuhrmann, L., et al. 2013, *A&A*, 552, A11
- Rau, A., Schady, P., Greiner, J., et al. 2012, *A&A*, 538, A26
- Richards, G. T., Myers, A. D., Gray, A. G., et al. 2009, *ApJS*, 180, 67
- Romani, R. W., Sowards-Emmerd, D., Greenhill, L., & Michelson, P. 2004, *ApJ*, 610, L9
- Sbarrato, T., Ghisellini, G., Nardini, M., et al. 2012, *MNRAS*, 426, L91
- Sbarufatti, B., Treves, A., Falomo, R., et al. 2005, *AJ*, 129, 559
- Schlegel, D. J., Finkbeiner, D. P., & Davis, M. 1998, *ApJ*, 500, 525
- Sesar, B., Ivezić, Ž., Lupton, R. H., et al. 2007, *AJ*, 134, 2236
- Shaw, M. S., Romani, R. W., Cotter, G., et al. 2013, *ApJ*, 764, 135 (shaw13)
- Sikora, M., Begelman, M. C., & Rees, M. J. 1994, *ApJ*, 421, 153
- Skrutskie, M. F., Cutri, R. M., Stiening, R., et al. 2006, *AJ*, 131, 1163
- Sowards-Emmerd, D., Romani, R. W., Michelson, P. F., & Ulvestad, J. S. 2004, *ApJ*, 609, 564
- Sowards-Emmerd, D., Romani, R. W., Michelson, P. F., Healey, S. E., & Nolan, P. L. 2005, *ApJ*, 626, 95

- Stecker, F. W., Malkan, M. A., & Scully, S. T. 2012, *ApJ*, 761, 128
- Tanaka, Y. T., Cheung, C. C., Inoue, Y., et al. 2013, *ApJ*, 777, L18
- Tavecchio, F., Maraschi, L., & Ghisellini, G. 1998, *ApJ*, 509, 608
- Urry, C. M., & Padovani, P. 1995, *PASP*, 107, 803
- Urry, C. M., Scarpa, R., O'Dowd, M., et al. 2000, *ApJ*, 532, 816
- Voges, W., Aschenbach, B., Boller, T., et al. 2000, *IAU Circ.*, 7432, 3
- White, R. L., Becker, R. H., Helfand, D. J., & Gregg, M. D. 1997, *ApJ*, 475, 479
- Wild, V., & Hewett, P. C. 2005, *MNRAS*, 358, 1083
- Wright, E. L., Eisenhardt, P. R. M., Mainzer, A. K., et al. 2010, *AJ*, 140, 1868
- Zhang, J. J., Fan, Y. F., Chang, L., Wang, C. J., & Yi, W. M. 2012, *Astronomical Research & Technology* (Chinese), 9, 411